A review of train aerodynamics Part 1 – Fundamentals

Baker, Christopher

A Review of Train Aerodynamics

Part 1. Fundamentals

Chris Baker

Birmingham Centre for Railway Research and Education

School of Civil Engineering

Gisbert Kapp Building, University of Birmingham, Edgbaston, Birmingham, United Kingdom, B15 2TT

Abstract

This paper is the first of a two part review of train aerodynamics. After an initial introduction and broad survey of train aerodynamic issues, and a discussion of measurement, modelling and computational techniques, the nature of the flow around trains is considered – in the open air, with and without crosswinds, and in confined geometrical situations and tunnels. The flow in different regions around the train is described and the main flow features outlined. Part 2 of the paper will then consider a number of issues that are of concern in the design and operation of modern trains based on this description of the overall flow field.

1. Background and history

In very broad terms, train aerodynamic effects increase in severity with the square of the speed of the train, and historically came to become of concern as the speed of passenger trains increased beyond around 100 km/hr. In the first instance attention was paid to reducing the aerodynamic drag of trains, both to reduce fuel consumption and to enable higher speeds to be achieved. As long ago as 1938, tests were being carried out at the London, Midland and Scottish Railway Research Centre at Derby to measure the aerodynamic drag of Coronation class steam engines, and to investigate smoke dispersion around the locomotive (1). But a whole series of other issues rapidly became apparent as train speeds of 200 km/hr or more became common. The existence of severe pressure transients in tunnels that caused considerable passenger discomfort was investigated in both Europe and Japan (2). Indeed in the UK aerodynamic speed limits were imposed on some narrow Victorian tunnels such as that at Patchway in south west England where the pressure transients were found to be very severe at higher train speeds. The stability of lightweight trains in high winds became an area of concern particularly in the context of the work on the GB Advanced Passenger Train (3). Figure 1 shows some 1/5th scale model tests that were carried out on a military test track to measure the cross wind forces on this train (4). Accidents involving pantograph dewirement in high winds also became increasingly common (5) with methods being derived for determining the correct spacing between cable supports to minimise this problem. The effects of high wind velocities in train slipstreams on workers at the trackside, passengers waiting on platforms, and, most particularly pushchairs holding small children, caused largely by aerodynamically rough freight trains also became apparent (6). As speeds increased still further to 300 km/hr and beyond these issues became of increasing concern, and yet a further set of issues became apparent – sonic booms from the exits of railway tunnels (7), failure of trackside structures such as noise barriers due to fatigue loading by train pressure transients (8) and the lifting of large ballast particles beneath trains causing damage to both trains and track (9) – see figure 2 for an example of track damage due to the crushing of ballast between wheel and track. Today the range of aerodynamic issues that need to be taken into account in the design process for new trains and new routes is extensive. In Europe, considerable work has been carried out over recent years to develop standards and codes to aid in this process, and this has resulted in a series of codes of practice produced by CEN (10) (11) (12) (13) (14) (15), and aerodynamic provisions in the Technical Standards for Interoperability (TSI) for both Rolling Stock (16) and Infrastructure (17). These will be referred to extensively in what follows.

The problems thus having been set out, obviously questions arise concerning how these issues can be addressed. It is the aim of this paper to consider a number of the issues relevant to modern trains. At the start however it needs to be made clear that a full understanding of the aerodynamic

behaviour of trains is very difficult to achieve for a variety of reasons – the wide range of possible train shapes, sizes and configurations; the fact that trains run in a very "dirty" aerodynamic environment over rough ground, often with highly turbulent cross winds, with a large number of trackside constraints of different types such as cuttings, overbridges, stations etc. As will be pointed out below, a boundary layer develops along the length of a train, and by the time this boundary layer reaches the end of the train, such boundary layers can have lateral dimensions similar to the size of the train itself, very different from the thin boundary layers on aeroplanes. Whilst these effects do not of course make life easy for the investigator, they do result in a fascinating series of practical and intellectual challenges for those involved in the field of train aerodynamics

This paper is the first part of a two part review of train aerodynamics. In this part we specifically consider the fundamental flow field around trains. We will continue in section 2 with a discussion of the different experimental and computational techniques that are available for the study of train aerodynamics. In sections 3 to 5 of this paper, the fundamental flow around trains is described – in the open air with no wind, in cross wind conditions in the open air, and in physically constrained environments and tunnels. The approach that is taken in this paper is that if the various practical issues are to be fully understood, then this can only come from an understanding of the flow field around the train. Some brief concluding comments are made in section 6.

Before moving on however, a number of other comments need to be made. Firstly it will become obvious that this review is from a mainly British perspective, although it will contain much information from non-British sources. This of course simply reflects the author's background and experience. Secondly it should be noted that this is not the first review of train aerodynamics. Earlier reviews have been presented by Gawthorpe (2), (5), (6), Schetz (18), Ragunathan (19) and a review, restricted largely to a consideration of the flow field around trains, by the author himself (20). The material presented in these reviews will be frequently drawn on in what follows. Thirdly, this review is concerned with conventional (wheel / rail) train systems only – Magnetic Levitation and Evacuated Tube transport are not considered – the interested reader should consult (18) for further discussion of the aerodynamics of the first of these and (21) for the latter. Finally there are a number of technical issues that are also excluded from the discussion – primarily aero-acoustic issues and pantograph dynamics.

2. Tools and techniques

There are essentially four methodologies that can be used to study the aerodynamic behaviour of trains – full scale testing, model scale testing, computational fluid dynamics and analytical methods. We consider each of these in turn in what follows.

Full scale testing is, as one might expect, complex and difficult. The organisational aspects of such trials – in terms of train, track and human resource availability is far from straightforward, and, as noted above the aerodynamic environment is "dirty", and the interpretation of results thus made difficult. Nonetheless full scale measurements are real, with no modelling assumptions, and for all their difficulty, form a base line against which the results all other techniques can be judged. The standard tools used for such measurements are two or three component sonic anemometers to measure wind and slipstream speeds (figure 3), solid state pressure transducers to measure pressure time histories (figure 4), and, where required, strain gauges and load cells to measure aerodynamic forces (figure 5). These all need to be sampled at frequencies of around 100 samples / sec, and care needs to be taken with positioning and calibration. Measurements also need to be made of meteorological conditions, using standard meteorological instruments, and train position and velocity, usually using light gates mounted to the track side that can identify the passing of the train (figure 6) (22). It is usually found that the results that are obtained are variable from train pass to train pass for a number of reasons – slight changes in train geometry (this is particularly the case with freight trains where the consists can be very variable); changes in environmental conditions, such as cross winds, and, perhaps most importantly, because each set of measurements is a realisation, from the point of view of a stationary observer, of a very unsteady turbulent flow field around the train. This has led to the concept of ensemble averaging of experimental results (23) – the determination of time histories of velocity or pressure for a large number of train passes, non-dimensionalising the measured parameters for each run, and then averaging the results for each of the runs at discrete time / distance positions relative to the nose of the train. Typical results for such a process, for slipstream velocities are shown in figure 7 from the measurements made on the S103 train for the recent AeroTRAIN experiments (24). The individual runs and the ensemble average and standard deviations are shown. The run by run variation can be seen to be very significant indeed – but this is largely a function of the physics of the phenomenon rather than any experimental error. Note that there are some flow regions where the uncertainty is very large in relation to the mean value – in particular the near wake of the vehicle. In general it is found that around 20 runs are required to get stable averages of velocity fields, but only a small number (around 3) to obtain stable averages of pressure transients.

Physical modelling of trains has the advantage over full scale testing in having controlled environmental conditions, but does result in a considerable number of modelling issues. If a conventional wind tunnel is used, the train will need to either be mounted on the wind tunnel floor on some simulation of railway track or on a suitable ground board, or above a moving belt. The high length / height ratio of the train results in a number of issues – first there is the practicality of fitting a full model train into a wind tunnel and of holding it in position above a moving ground plane (25). For stationary models, as noted above, the boundary layer growth along the ground plane is considerable and at the rear of the train represents unrealistic conditions. Then of course there is the issue of scale (or Reynolds number) effects (see the next sections for a dimensional analysis of the problem), as the model scale trains have values of Reynolds number much lower than would be found in reality. For experiments with cross winds, wind tunnel tests on the leading vehicles are used extensively and the methodology is well documented (15), (26). Such tests will be discussed in more detail in Part 2 , but it will be clear that standard low turbulence wind tunnel tests with a static model do not fully model atmospheric conditions, or the relative motions between train and ground and train and air. These points being made, wind tunnel experiments on trains are usually conducted with standard velocity, pressure and force measuring equipment, using normal wind tunnel methodology and practice.

There is however another type of experimental technique that can be used for train aerodynamics - the moving model method, in which a moving model of the train is fired along a test track. Clearly this simulates the ground conditions more accurately than the wind tunnel, but at the expense of model complexity. A number of such rigs now exist around the world – for example at the University of Birmingham in the UK, DLR in Germany, JRRI in Japan, and Central South University at Changsha in China, and essentially consist of a firing mechanism of some sort, and acceleration section, a working section and a braking section. The rigs are usually of the order of 100 to 200m in length. Photographs of the UOB TRAIN Rig facility are shown in figure 8. For tests on trains in the open air, such rigs can make accurate measurements of train slipstreams and pressure transients that compare well with full scale experiments – figures 9 and 10 (27). They have also been used extensively for measurements in tunnels, where pressure time histories are required. In Part 2 it will be shown that for these tests to be representative of the full scale situation, models need to be run at the correct Mach number which implies full scale speeds, and moving model rigs can be used at speeds of up to 80 to 100m/s for this purpose. Tests with cross winds can also be made if a suitable cross wind generator is placed next to the track (see figure 11 for example), but here the measuring crosswind pressures and forces on moving trains results in complex and difficult experiments (28), with on board balances or pressure transducers that need to withstand the high accelerations and

decelerations involved. In general the measurements on such rigs can be made with standard wind tunnel equipment, although very high sampling rates are required, particularly at the higher model speeds – up to 10000 samples / second.

In recent years, CFD modelling has come to be used more and more in the study of train aerodynamics, and such techniques have a great deal to offer in terms of the detail that they can provide concerning the flow field around trains – usually to a much higher resolution than is available from experimental data. There are major challenges to the routine use of CFD in train aerodynamics however – primarily the length / height ratio of the train already mentioned, makes gridding difficult, with high resolution grids needed along the entire train surface. However provided normal CFD best practice is followed (29) in terms of mesh size, resolution, convergence etc., then useful results can be obtained. Different types of turbulence model are applicable for studies of specific regions around the train. The flow around the noses of reasonably streamlined trains will be seen in the next section to be essentially inviscid, and simple Boundary Element Methods can be used for the study of the velocity and pressure changes in such regions (30) – figure 12. For more complex nose shapes or for studies around the leading cars of trains, RANS methodology is more appropriate, and can deal with distorted flows and limited separation regions. Such methods can also be used to investigate the effects of cross winds at low yaw angles (31) – figure 13. However difficulties occur in regions around the train where the boundary layer thickness is large (i.e. some distance from the nose), or where there are large scale separations (i.e. in the train wake or for high yaw angle cross wind conditions). In such circumstances, the essentially steady RANS methods should be used with the greatest circumspection. Unsteady flow methods such as LES and DES are required here that can properly simulate the unsteady flow fields (32) – figure 14. However it should be noted that the Reynolds numbers that can be achieved in such simulations are very low at present, and any results should be used with care. However such methods show great promise for the future.

Finally we consider the use of analytical methodologies. Whilst the modelling and computational tools outlined above offer ways of investigating aerodynamic issues in detail, there are a number of circumstances where straightforward analytical methods have considerable utility. This is particularly the case in the consideration of tunnel flows, where one dimensional analyses of the propagation of pressure waves along the tunnel are usually quite sufficient for most practical issues (33). These can lead to some simple and easy to apply formulae for, for example, initial pressure rises in tunnels. These are summarised in the CEN code (14).

3. The flow around trains in the open air in low wind conditions

3.1 Basic parameters

The basic parameters that describe the flow field around a train are the velocity and pressure fields on and around the train – $u_x(x,y,z)$, $u_y(x,y,z)$, $u_z(x,y,z)$ and $p(x,y,z)$. u_i *is* the components of velocity in the *i* direction; *x* is the co-ordinate in the train direction of travel and will in general be measured from the train nose. *y* is the lateral direction, and will be measured from the centre of the track. *z* is a vertical direction, measured above ground level. The parameters on which they could be expected to depend are the train height *h*, the train width *b*, the train length *L*, the length of the nose *l*, the height of the under body of the train above the track bed *t*, the roughness of the train *k*, which may be defined as the standard deviation of the profile area variation along the length of the train, the train velocity *v*, and the parameters that define the properties of air – density ρ and viscosity μ. As is normally the case in aerodynamic studies, it is convenient to express these in a dimensionless form, and in what follows we will express the velocity and pressure fields in dimensionless forms as u_i/v and $C_p = p/0.5\rho v^2$. These will be taken to depend upon the dimensionless ratios *b/h, L/h, l/h, t/h and k/h*, and the basic aerodynamic scaling parameter, the Reynolds number $Re=\rho vh/\mu$.

3.2 Flow regions around a train

Figure 15 shows the ensemble average horizontal velocities (the vector sum of u_x and u_y) normalised with train speed, measured at the side of an ICE-2 train during the RAPIDE experiments (34). It proved to be convenient to divide the flow field thus measured into a number of different regions as follows.

- The nose region, extending from upstream of the train to around 5 to 10m behind the nose, where figure 15 shows there is a large velocity peak.
- The boundary layer region of the train, extending from the end of the nose region to the end of the train (at x=364m). Figure 15 shows the gradual development of the flow in this region, with the measurements made furthest from the train having low velocities until the boundary layer grows sufficiently for the measurement point to be within the boundary layer.
- The near wake region extending around 100m behind the train, where there is a large velocity peak. This is the region in which, for some trains, coherent flow structures exist, including longitudinal vortices.
- The far wake region, extending from the end of the near wake region, in which the velocities gradually decay to zero.

In what follows we will consider each of these regions in turn. We will also consider two further regions of flow – beneath the train (the underbody flow) and flow above the roof. Before we proceed however, it is convenient to set out here figures similar to figure 15 for a range of different train types. This is done in figure 16 for the Velaro S103 train – a 200m long high speed passenger train with a streamlined but rounded nose and tail (24); in figure 17 for an S100 TGV, which is again a 200m long train but with a more pointed streamlined nose (24); in figure 18 for the Talgo S102, which has a beak like nose and tail; in figure 19 for the S252 locomotive plus trailing coaches (24); in figure 20 for the 200m long HST, a rather blunt nosed train, again 200m long (previously unpublished data); and in figure 21 for model scale freight train measurements, with a blunt ended Class 66 locomotive and a freight flats partially loaded with containers (35). These reflect the broad range of train types and will be considered further in what follows.

3.3 Nose region

The flow around the nose of many trains is largely invisicid with low turbulence, and the pressure and velocity variations are well defined. Typical pressure variations have been shown in figure 9 above for the ICE-2 (27). A large positive peak in pressure is followed by a negative peak, which is typical of most trains. Similar results are shown for two HST configurations (2 power cars plus 7 coaches and 2 power cars plus 8 coaches) in figure 22 and a model scale freight train experiments in figure 23. Now, it is clear from figures 15 to 21 that there are also large peaks in horizontal velocity near the nose. However this large peak is due to variations in the velocities in both the *x* and *y* directions. An example of this is shown in figure 24 for the Velaro S103 train (24). The *x* component of velocity u_x follows the form of the pressure variation (indeed a simple application of the energy equation suggests that $u_x/v = C_p/2$), but there is also a strong lateral velocity peak u_y in the positive *y* direction i.e. away from the train. If only overall horizontal velocity measurements are made (such as for example with hot wires), then this lateral velocity will dominate and the negative u_x component peak will not be observed. Figures 15 to 21 show that, very broadly at a fixed distance from the side of the train, the size of the overall normalised velocity nose peaks increase with the bluntness of the train, with values of between 0.05 and 0.1 for passenger trains, and very much higher for blunt freight trains. Similarly the results for ETR trains with different nose lengths shown in figure 12 (30) show how the pressure coefficient changes significantly with nose bluntness i.e. the velocity peak increases as l/h decreases. Finally it should be noted from the locomotive / carriage results of figure 19, that for this case the ensemble shows a peak close to the nose of the train at the discontinuity between the locomotive and the trailing coach, indicating highly disturbed flow in this area.

3.4 Boundary layer region on train sides

As might be expected, along the side and roof of trains there is the development of a large scale turbulent boundary layer. This boundary layer is however far from being two dimensional with a component of velocity up or down the train wall, and divergence or convergence of velocity over the top of the train (36). The development of the boundary layer can be clearly seen in figures 15 to 21. The detailed measurements of figure 15 for the ICE-2 also the boundary layer velocity profiles to be plotted, and typical results are shown in figure 25 (34). Perhaps the most important point of note is the scale of the boundary layer – towards the rear of the train the size of the layer is comparable with the width / height of the train itself. Figure 26 shows plots of the displacement thickness, form parameter, turbulence intensity and turbulence integral length scales along the same train (34). It can be seen that the displacement thickness in general increases along the length of the train, although the nature of this increase is different at full scale and model scale, with a large initial value at full scale, presumably due to some flow disturbance around the nose. The form parameter is lower than for an equilibrium boundary layer, and reflects the essential three dimensionality of the flow. The turbulence intensity (in the stationary frame of reference) is fairly constant along the train, although with very great fluctuations, with values of around 0.1. The autocorrelation function is also shown from which integral length scales (in the longitudinal flow direction) of approximately 4.0m can be calculated.

Boundary layer measurements were made during the RAPIDE experiments (37), but this time using a train mounted laser anemometer. Typical results are shown in figure 27 for measurements made on an ICE-2 and a TGV, 194m from the train nose. The boundary layers can be seen to be over 1m thick, although the velocities at that distance (relative to the ground) are smaller than would be expected from the ground based measurements of figure 25, suggesting a thinner boundary layer at this point. The difference is probably due to the fact that the ground based measurements were made significantly closer to the ground than the train based measurements, and thus reflect the increased roughness caused by bogies etc. Some equivalent stationary wind tunnel tests are also shown in figure 27 – it can be seen that these results indicate a much thinner boundary later than was actually measured, implying that the wind tunnel tests do not fully capture all the physical energy consuming processes found at full scale. This is consistent with the difference between the model scale and full scale displacement thickness measurements shown in figure 26.

Within the train boundary layer in low wind speed conditions, the pressure coefficients are usually close to zero on average. However if there are significant discontinuities along the train – such as pronounced bogies or gaps between freight containers, then these have a distinctive pressure signature – see for example figures 22 and 23 for Class 43 HSTs and container trains.

3.5 Near wake

The near wake is the most complex of the flow areas around the train, and can take on a variety of forms depending on the precise shape of the train. A typical pressure signature can be seen in figure 22 for an HST – these show the reverse of the nose situation with a negative peak followed by a positive peak. These are in general less severe than the nose peaks. For blunt ended trains, there seems to be little evidence of flow structure, and large scale separations occur. However for more streamlined trains, there is evidence of the existence of a pair of longitudinal trailing vortices behind the train - see the computational results figure 28 (20) and the experimental PIV results of figure 29 (23). These can result in very high velocities in the train wake – see the wake peaks in figures 15 to 20 – and thus low pressures. Figure 30 shows recent TRAIN Rig measurements around a 4 car ICE-2 model made with Cobra (multi-hole) probes that give both pressure and velocity outputs. The probes were placed at the TSI measurement position at just above track height, 3.0m from the track centre line over a deep ballast shoulder. It can be seen that the peak in the ensemble velocity corresponds to a second minimum in the pressure trace – presumably within the longitudinal trailing vortex. There is also evidence that these vortices can be unsteady. The time dependent CFD results of figure 31 illustrate this well (38). Such unsteadiness was also observed in the full scale data of (34), where the individual runs of the ensemble only intermittently showed a wake peak, or showed double or triple peaks. This led the authors to suggest that the technique of ensemble averaging might not be wholly suitable to analyse such structures. That being said the Strouhal numbers of the CFD simulation (38) and the full scale experiments (34), defined as oscillation frequency x body height / train velocity, were reasonably similar – 0.14 for the former and 0.11 for the latter.

3.6 Far wake

In the far wake behind trains, there is little pressure variation and a gradual reduction in the flow velocities – see figure 32 which shows the velocity decay behind the Velaro S103 (24). The nature of this decay was analysed in some detail by the author in (39). However that analysis was primarily aimed at short cars and was not wholly applicable for trains. In (24) a much simpler approach was adopted using a simple power law form, with the velocity being taken to be proportional to (*distance from the end of the train*)^{n}. For a wide range of trains the exponent *n* was found to be close to 0.5.

3.7 Underbody flows

A number of authors have made measurements of velocities and pressures beneath trains in recent years, mainly in investigations of the ballast flight problem (see Part 2). Typical pressure and velocity measurements, for the Eurostar Class 373 train (which is essentially a TGV) are shown in figures 33 and 34 (9). Again these are shown in the form of ensemble averages which masks rather large unsteadiness, particularly in the velocity measurements. The nose pressure peak is very obvious, but the nose suction peak is somewhat obscured by high levels of unsteadiness beneath the train. The velocity rises to a constant level within the first car along the train. It can be seen that there is relatively little change in pressure or velocity along the train, although it is clear that the individual bogies can be discerned from the pressure plots. The Eurostar is composed of two units coupled together, and the position of this coupling can also be discerned in the centre of the trace. The velocity rises to an equilibrium value, and remains at this value during the passage of the train. At the end of the train the characteristic suction / pressure peak can be seen. Other authors have measured velocity and pressure variations across the underbody gap – see figure 35 for example (40). These generally show a characteristic "S" shape, with a point of inflection at about half height. Detailed experiments were carried out using PIV in water towing tank to measure the flow beneath a generic train with different underbody roughnesses (41) i.e. the ratio k/t – figure 36. These show the evolution of the profile along the length of the train, and indicate the significant effect of underbody roughness. However there is little data available that shows how the underbody flow field varies with k/t and t/h.

3.8 Flow over the roof of the train

The flow over the roof of a train is particularly important in the consideration of the aerodynamic importance of pantographs. In view of this, it is surprising that, very few detailed flow measurements have been made over the roof of trains. The only data sets that have been obtained for this region of small scale model results from the 1980s on the HST (36), a short series of measurements made on the TRAIN Rig above a four car ICE2 model (23), and the recent measurements by the author and his colleagues of flow at roof height, and to the side of, full scale HSTs, made as part of an investigation concerned with the electrification of the GB Great Western Main Line. The results of the model scale tests are to some degree contradictory with the results of (36) showing larger displacement thicknesses on the roof of the train than on the side, and the results of (23) showing the opposite effect (20). Both however illustrate the significant three dimensionality of the boundary layer development along the train side and roof. The results of the full scale experiments have already been shown in figure 20 (as the "rooftop" tests), again as an ensemble average of a large number of runs. The interesting point to note from this figure is the

large peak in velocity along the first vehicle of the train, presumably caused by some large scale flow structure downstream of the nose. This phenomenon merits further investigation, as indeed does the boundary layer development over the roof of the train in general.

4. The effects of wind

As might be expected the effect of cross winds on the flow around trains are considerable, and of some practical importance. Near the ground the natural wind is highly turbulent and sheared, and is significantly influenced by local topography. In the simplest case above flat ground, the mean velocity profile $u(z)$ is logarithmic and defined by a surface roughness height, z_0, and surface friction velocity, u_*, as follows (42)

$$u(z) = u_* \ln\left(\frac{z}{z_0}\right) \quad (1)$$

The turbulence is defined by the turbulence intensity

$$I = \frac{\sigma(z)}{u(z)} = 1/ln\left(\frac{z}{z_0}\right) \quad (2)$$

where $\sigma(z)$ is the standard deviation of the velocity fluctuations at height z above the ground. The scale of turbulence close to the ground is not well defined, but seems to vary linearly with height. Similarly the wind spectrum near the ground is ill defined below around 5m height, but will be heavily influenced by local effects. However the open flat ground case is an abstraction and rarely occurs in practice. The effect of typical railway structures, such as embankments and bridges can have a major effect on the wind field experienced by the train. For example above an embankment, it is conventional wisdom to apply the embarrassingly named "Baker hypothesis", which suggest that the component of wind normal to the embankment experiences a speed up as it passes over the embankment, whilst the component of the wind along the embankment does not change (although it should be noted that the author has recently emphasised the small amount of data on which this is based (20)).

Figure 37 shows a vector diagram of wind and train velocities. The wind velocity relative to the train, *V*, is given by

$$V^2 = ((u(h)cos(\beta) + v)^2 + (u(h)sin(\beta))^2) \quad (3)$$

where *u(h)* is the mean velocity defined at some reference height *h*, often taken as 3m, *v* is the train velocity, β is the wind direction. The angle of the wind relative to the train is given by the yaw angle ψ.

$$\tan(\psi) = \frac{u(h)\sin(\beta)}{u(h)\,cos(\beta)+v} \quad (4)$$

Thus to the parameters listed in section 3.1 of importance for trains in the open area, we need to add, β, ψ, and h/z_0. Based on the above expressions it is instructive to consider the wind as seen by the moving train. This is illustrated in figure 38 below, for a 20m/s cross wind normal to the track,

with a turbulence intensity given by the above equation. It is clear that as the train speed increases the velocity profile seen by the train becomes flatter and the effective turbulence intensity becomes lower. This has implications for wind tunnel tests – see section 2 and Part 2. The wind spectrum relative to the vehicle can also be determined using the methodology of Cooper (43), and this will be seen to be of importance in the study of the dynamics of rail vehicles in cross winds,

For small yaw angles of the order of 0 to 5 degrees i.e. low cross winds, the flow field around a train can be modified in small but potentially significant ways. For example the boundary layer development along the train can be skewed, with a thicker lee side boundary layer and a thinner windward side boundary layer. The near wake seems to be particularly sensitive to small cross winds however. The AEROTRAIN project slipstream measurements (24) show that the ensemble averages of velocities can be significantly changed by even low cross winds – see figure 39 for example. This is presumably because the longitudinal trailing vortices in the wake are moved laterally (towards or away from the measuring instruments) in cross wind conditions. At larger yaw angles, from 5 to 40 degrees it is generally accepted that longitudinal trailing vortices form on the leeward side of streamlined trains. Early work at Cambridge (44), (45) studied this vortex pattern in detail around an idealised train shape above a ground board and revealed a complex vortex structure along the train (figure 40). Similar flow patterns have been revealed in more recent CFD calculations (figure 13) (31). The extent to which such complex structures exist in highly turbulent natural conditions, with turbulent winds and complex train geometries, is however debatable. At the higher yaw angles (above 60 degrees), which are only relevant for slow or stationary trains, such evidence as exists suggest that the flow field around trains more closely resembles that around a prism normal to the flow, with large scale separation and some degree of vortex shedding, although the latter is inhibited by the effect of the ground (20). These major changes in flow field of necessity have a significant effect on the pressure field around trains. Figure 41 shows how the pressure develops around different sections of a multiple unit train for yaw angle of 45 and 90 degrees. Perhaps the most notable feature is the large suction peak around the nose of the train in particular and around the windward top edge of the train in general.

5. Flow constraints and tunnels

Whilst the discussion of the last two sections concerning trains in the open air is useful in setting the base conditions for considering the flow around trains, it is an obvious fact that such conditions are very often compromised in practice, with the flow around trains being constrained in one way or another – either through the track formation itself (cuttings and embankments) or by the presence of trackside structures, such as wall, stations and bridges, or in the extreme case by tunnels of various lengths. In this section we will consider the effect of such constraints on the pressure and velocity fields around trains.

A recent study has measured the pressure loads on a variety of trackside structures such as hoardings, over bridges, station canopies etc. (47) (48) These tests were aimed at determining the loading on such structures for UK gauging conditions and will be discussed further in Part 2. Here however we use them to illustrate the nature of the changes to the pressure fields around trains. Figure 42 shows the pressure measured on trackside and platform mounted hoardings, and figure 43 shows a similar figure for the pressures on 19m, long, 4.5m high overbridges, for three different passing train types – a relatively streamlined Class 390 train, a blunt ended Class 158 multiple unit and a Class 66 freight locomotive. These pressure time histories have the same form as those measured in the open air and shown in figures 22 and 23. The most important thing to notice however is the magnitude of the peaks – significantly higher than for the open air case, and showing a great variability with the train type. Indeed it is straightforward to show that the pressure coefficient on a wall ought to be a factor of 2 higher than in the free stream at an equivalent distance away from the train for idealised flow conditions. In similar earlier experiments tests were carried out to measure pressure loading measurements on the surface of train models and they were passed by moving models (49). Not surprisingly the investigators found that the pressures increased as train spacing decreased – see figure 44. Essentially the effect of flow constraints of this sort is to increase the magnitude of the head pressure pulse.

In a recent PhD study, Gilbert (50) (51) (52) has carried out a systematic study of the effect of flow constraints on both pressure and velocity fields, for single and double walls next to the train, and short and long tunnels of different types, using moving model techniques. Some examples of this work are shown in figure 45 for pressure measurements and figure 46 for velocity measurements. Consider first the results of figure 45 which shows the variation in wall pressure caused by the passage an ICE-2 train through a rectangular box tunnel, with different degrees of “ventilation”. Whilst the pressure transients at the front and end of the train remain visible throughout, their magnitude increases as the level of constraint increases (i.e. ventilation opening size decreases), and the form of the peaks changes to the form that will be shown below is typical of flow through a fully

sealed tunnel. For the more constrained cases the pressure shows significant oscillatory variations, due to pressure waves passing along the tunnel. This is again described below. Figure 46 for the velocity profiles for various types of constraint ranging from the open air case to a long tunnel case, shows a major increase in velocity near the train and in the wake as the level of constraint increases. For the fully enclosed tunnel case, there can be seen to be a velocity in the tunnel before the train passes as would be expected.

The distinctive nature of flow through tunnels has already been mentioned above. The basic phenomenon that makes this different to flow in the open air is the existence of pressure waves that pass along the tunnel and reflect from the end. As a train enters a tunnel a positive (compression) pressure wave is generated that moves along the tunnel ahead of the train, and reflects at the far end of the tunnel as a negative (expansion) wave. As the tail of the train passes into the tunnel a negative expansion wave forms that passes over the train, and itself reflects as a positive pressure wave. Depending on the length of the train and the length of the tunnel the combination of these waves can very complex indeed. This is usefully summarised in figure 47 (12), which shows the complex pattern of waves that exists in a single track tunnel. Of particular importance is the steep initial pressure rise as the train nose entered, followed by the more shallow pressure rise due to the frictional effects of the passage of the train. The pressure patterns observed by a stationary observer and an observer on a moving train are also shown. For long tunnels, friction effects become important, and there is some attenuation of the pressure wave magnitudes. For long tunnels running on a gradient, there may also be a significant pressure difference between the two ends of the tunnel due to the height difference, and this difference will be superimposed upon the pressure transients shown in the figure. The even more complex situation of two trains passing in a tunnel is summarised in the same way in figure 48 (12). Such pressure time histories, from both the viewpoint of the stationary and moving observer, are of course very dependent upon the relative entry times of the two trains into the tunnel.

One other issue concerning the nature of the pressure transients needs to be mentioned above, although its full implications will not be considered until Part 2. It has been noted that there will be some attenuation of the pressure wave due to friction in long tunnels. The primary cause of such friction is the nature of the ballasted track. Not only does this cause an attenuation of the magnitude of the wave, but it also results in a spreading of the wave i.e. the waves become less steep in terms of distance along the tunnel. However for other track forms – and in particular concrete slab track – the effects of friction are much reduced, and there is the potential for the wave fronts to steepen. When such waves exit from the tunnel, there is the potential for external micro-pressure waves (better known as sonic booms) to form (7).

6. Concluding remarks

This paper has presented a description of the flow field around trains in the open air with and without crosswinds and in confined situations such as cuttings and tunnels. It has been shown that a number of different flow regions around the train can be identified, and the nature of the flow in these regions has been set out. The modifications to these flow patterns by cross winds and flow confinement have been discussed. In part 2 of this paper a number of train aerodynamic applications will be discussed using this knowledge of the flow field as the basis for the discussion.

Acknowledgements

It will be evident from the reference list that the author is indebted to a large number of industrial and academic colleagues and research students past and present for much of the information that is included in this paper, and it is simply not possible to name them all. Their contribution is gratefully acknowledged. However the author would specifically like to acknowledge the part played by Roger Gawthorpe, former Head of Aerodynamics Research at British Rail, and the one who first introduced him to the fascinating subject of train aerodynamics.

Figures from other sources

The author would like to acknowledge the permissions given by various organisations and individuals to reproduce figures for this paper. These are as follows. Figure 1 © National Railway Museum and SSPL, http://www.nrm.org.uk/; Figures 2, 5, 7, 13, 15, 16, 17, 18, 19, 20, 24, 25, 26, 28, 29, 32, 33, 34, 39, 42, 43 Reproduced with permission from Sage Publications Ltd.; Figure 6 Reproduced with permission from the authors; Figure 12 Permission granted by Elsevier under license number 3290160913713; Figure 14 Permission granted by Elsevier under license number 3258160010706; Figure 27 Reproduced with permission from the authors; Figure 31 Copyright Wiley-VCH Verlag GmbH & Co. KGaA. Reproduced with permission; Figure 35 Reproduced with permission from WCRR; Figure 36 Reproduced under the Creative Commons License held by TU Berlin; Figure 40 Permission granted by Elsevier under license number 3258160251106; Figures 47, 48 Permission to reproduce extracts from British Standards is granted by BSI Standards Limited (BSI).

References

1. Bellwood J E, Jenkinson D (1976) Gresley and Stanier: A Centenary Tribute. London: Her Majesty's Stationery Office. ISBN 0-11-290253-7.
2. Gawthorpe R G (1978) Aerodynamics of trains in tunnels, Railway Engineer International 3, 4, 41-47
3. Cooper R K (1979) The probability of trains overturning in high winds, Proceedings 5th International Conference on Wind Engineering, Fort Collins, CO, USA 2, 1185
4. NRM (2013) Aerodynamic testing of small model of APT at Pendine, NRM Archive, http://www.nrm.org.uk/ourcollection/photo?group=BR%20Research%20Derby&objid=1999-7442_BR_RCP_58, accessed 26/7/2013
5. Gawthorpe R G (1978) Aerodynamic problems with overhead line equipment, Railway Engineer International, 3, 4 38-40
6. Gawthorpe R G, (1978) Aerodynamics of Trains in the Open Air, Railway Engineer International, 3, 3, 7-12
7. Vardy A E (2008) Generation and alleviation of sonic booms from rail tunnels, Proceedings of the Institution of Civil Engineers - Engineering and Computational Mechanics, 161, 3, 107 –119
8. Friedl H, Reiterer M, Kari H (2011) Aerodynamic excitation of noise barrier systems at high-speed rail lines – Fatigue analysis, IOMAC'11 – 4th International Operational Modal Analysis Conference
9. Quinn A D, Hayward M, Baker C J, Schmid F, Priest J A, Powrie W (2010) A full-scale experimental and modelling study of ballast flight under high-speed trains, Proceedings of the Institution of Mechanical Engineers, Part F: Journal of Rail and Rapid Transit 224, 2 61-74, 10.1243/09544097JRRT294
10. CEN (2003), Railway Applications – Aerodynamics. Part 1 Symbols and Units, BS EN 14067-1:2003
11. CEN (2003), Railway Applications – Aerodynamics Part 2 Aerodynamics on Open Track E BS EN 14067-2:2003
12. CEN (2003) Railway Applications – Aerodynamics Part 3 Aerodynamics in tunnels BS EN 14067-3:2003
13. CEN (2009) Railway Applications – Aerodynamics Part 4 Requirements and test procedures for aerodynamics on open track, BS EN 14067-4:2005+A1:2009
14. CEN (2010) Railway Applications – Aerodynamics Part 5 Requirements and test procedures for aerodynamics in tunnels, BS EN 14067-5: 2006+A1:2010
15. CEN (2010) Railway Applications – Aerodynamics. Part 6 Aerodynamics Tests for crosswind assessment, BS EN 14067-6:2010
16. TSI (2008) "EU Technical Specification for Interoperability Relating to the 'Rolling Stock' Sub-System of the Trans-European High-Speed Rail System" HS RST TSI, 2008/232/EC
17. TSI (2008) "EU Technical Specification for Interoperability Relating to the 'Infrastructure Sub-System of the Trans-European High-Speed Rail System" HS RST TSI, 2008/217/EC
18. Schetz J A (2001) Aerodynamics of High Speed Trains, Annual Review of Fluid Mechanics, 33, 371-414, 10.1146/annurev.fluid.33.1.371
19. Raghunathan R S, Kim H D, Setoguchi T (2002), Aerodynamics of high speed railway train Progress in Aerospace sciences, 38, 6–7, 469–514, 10.1016/S0376-0421(02)00029-5
20. Baker C J (2010) The flow around high speed trains, Journal of Wind Engineering and Industrial Aerodynamics, 98, 6–7, 277–298, 10.1016/j.jweia.2009.11.002
21. Baron A, Mossi M, Sibilla S (2001) The alleviation of the aerodynamic drag and wave effects of high-speed trains in very long tunnels, Journal of Wind Engineering and Industrial Aerodynamics 89, 5, 365–401, 10.1016/S0167-6105(00)00071-4
22. Deeg P, Jonsson M, Kaltenbach H-J, Schober M, Weise M (2008) Cross comparison of measurement techniques for the determination of train induced aerodynamic loads on the trackbed. Proceedings of the conference on Bluff Bodies Aerodynamics and its Applications, Milano, Italy

23 Baker C J, Dalley S J, Johnson T, Quinn A, Wright N G (2001) The slipstream and wake of a high speed train, Proceedings of the Institution of Mechanical Engineers F Journal of Rail and Rapid Transit, 215, 83-99, 10.1243/0954409011531422
24 Baker C J, Quinn A, Sima M, Hoefener L, Licciardello R (2013) Full-scale measurement and analysis of train slipstreams and wakes: Part 1 Ensemble averages. Proceedings of the Institution of Mechanical Engineers, Part F: Journal of Rail and Rapid Transit, 10.1177/0954409713485944
25 Kwon H, Park Y, Lee D, Kim M (2001) Wind tunnel experiments on Korean high-speed trains using various ground simulation techniques, Journal of Wind Engineering and Industrial Aerodynamics, 89, 13, 1179–1195, 10.1016/S0167-6105(01)00107-6
26 Rail Safety and Standards Board (2009) Recommendations for Determination of Aerodynamic Rolling Moment Coefficient, GM/RC2542
27 Baker C J, Gilbert T, Jordan S (2013) The validation of the use of moving model experiments for the measurement of train aerodynamic parameters in the open air, Proceedings of the World Congress on Rail Research, Sydney, Australia
28 Dorigati F (2013) Rail vehicles in crosswinds; analysis of steady and unsteady aerodynamic effects through static and moving model tests. PhD thesis, University of Birmingham
29. Franke J, Hellsten A, Schlunzen H, Carisimo B (2010) The Best Practise Guideline for the CFD simulation of flows in the urban environment : an outcome of COST 732, The Fifth International Symposium on Computational Wind Engineering (CWE2010) Chapel Hill, North Carolina
30. Hermanns L, German Gimenez J, Alarcon E (2005) Efficient computation of the pressures developed during high-speed train passing events, Computers and Structures 83, 793–803
31 Diedrichs B (2003) On computational fluid dynamics modelling of crosswind effects for high-speed rolling stock, Proceedings of the Institution of Mechanical Engineers, Part F: Journal of Rail and Rapid Transit 217: 203, 10.1243/095440903769012902
32 Hemida H, Krajnović S (2010) LES study of the influence of the nose shape and yaw angles on flow structures around trains, Journal of Wind Engineering and Industrial Aerodynamics 98, 1, 34-46 10.1016/j.jweia.2009.08.012
33. Howe M S, Fukuda T, Maeda T (2000) Theoretical and experimental investigation of the compression wave generated by a train entering a tunnel with a flared portal, Journal of Fluid Mechanics 425, 111-132 10.1017/S0022112000002093
34. Sterling M, Baker C J, Jordan S C, Johnson T (2008) A study of the slipstreams of high speed passenger trains and freight train**s,** Proceedings of the Institute of Mechanical Engineers Part F: Journal of Rail and Rapid Transport. 222, 177-19, 10.1243/09544097JRRT133
35. Soper D, Baker C J, Sterling M (2013) Slipstream development of a container freight train, Proceedings of the International Workshop on Train Aerodynamics, Birmingham, UK
36. Brockie N J W, Baker C J (1990) The aerodynamic drag of high speed trains, Journal of Wind Engineering and Industrial Aerodynamics 34, 273-290, 10.1016/0167-6105(90)90156-7
37. RAPIDE (2001) Railway aerodynamics of passing interaction with dynamic effects. Synthesis report, Aerodynamics Workshop, Cologne
38. Schulte-Werning B, Heine C, Matschke G (2003) Unsteady wake characteristics of high speed trains. PAMM Proceedings Applied Maths and Mechanics 2, 332–333.
39. Baker C J (2001) Flow and dispersion in ground vehicle wakes, Journal of Fluids and Structures 15, 7, 1031-1060, 10.1006/jfls.2001.0385
40. Ido A, Saitou S, Nakade K, Iikura S (2008) Study on under-floor flow to reduce ballast flying phenomena. Proceedings of the World Congress on Rail Research, Seoul, South Korea, Paper S2.3.4.2.
41. Jönsson M, Haff J, Richard H, Loose S, Orellano A (2009) PIV Investigation of the flow field underneath a generic high speed train configuration, Euromech 509, External aerodynamics of railway vehicles, trucks, buses and cars, Berlin, Germany
42. Cook N J (1986) The Designer's Guide to Wind Loading of Building Structures: Static structures, Butterworths, ISBN-10: 0408008709

43. Cooper R K (1984) Atmospheric turbulence with respect to moving ground vehicles, Journal of Wind Engineering and Industrial Aerodynamics 17, 2, 215–238, 1016/0167-6105(84)90057-6
44. Mair W A, Stewart A J (1985) The flow past yawed slender bodies, with and without ground effects, Journal of Wind Engineering and Industrial Aerodynamics 18, 3, 301-328, 10.1016/0167-6105(85)90088-1
45 Copley J (1987) The three-dimensional flow around railway trains, Journal of Wind Engineering and Industrial Aerodynamics 26, 1, 22-52, 10.1016/0167-6105(87)90034-1
46. Baker C J, Sterling M, Bouferrouk A, O'Neil H, Wood S, Crosbie E, 2008 Aerodynamic forces on multiple unit trains in cross winds", Proceedings of the Conference on Bluff Body Aerodynamics and its Applications, Milano, Italy
47. Baker C J, Jordan S J, Gilbert T, Sterling M, Quinn A, Johnson T, Lane J (2012) Transient aerodynamic pressures and forces on trackside and overhead structures due to passing trains. Part 1 Model scale experiments, Journal of Rail and Rapid Transit, 228 36 – 69, 10.1177/0954409712464859
48. Baker C J, Jordan S J, Gilbert T, Sterling M, Quinn A, Johnson T, Lane J (2012) Transient aerodynamic pressures and forces on trackside and overhead structures due to passing trains. Part 2 Standards applications, Journal of Rail and Rapid Transit, 228 36 – 69, 10.1177/0954409712464859
49. Johnson T, Dalley S (2002) 1/25 scale moving model tests for the TRANSAERO Project. in TRANSAERO — A European Initiative on Transient Aerodynamics for Railway System Optimisation. 123-135, Notes on Numerical Fluid Mechanics and Multidisciplinary Design, 79, Schulte-Werning B, Gregoire R, Malfatti A, Matschke G (Eds.)
50. Gilbert T (2013) Aerodynamic effects of high speed trains in confined spaces, PhD thesis, University of Birmingham, UK
51. Gilbert T, Baker C, Quinn A (2013) Aerodynamic pressures around high-speed trains: the transition from unconfined to enclosed spaces, Journal of Rail and Rapid Transit, 227 (6), 608-62, 10.1177/0954409713494947
52. Gilbert T, Baker C, Quinn A (2013) Aerodynamic effects of high speed trains in confined spaces, Proceedings of the International Workshop on Train Aerodynamics, Birmingham, UK

Notation

In a publication such as this, with much material taken from published sources, it is difficult to achieve complete consistency of nomenclature. Nonetheless the major notation used is shown below. On many of the figures, information is given in the caption on the parameters shown in the figures.

b	Train width
C_p	Pressure coefficient
d^*	Boundary layer displacement thickness
h	Train height
H	Boundary layer form parameter
I	Turbulence intensity
k	Train roughness
l	Nose length or inter car gap length
L	Train length
n	wake decay exponent
$p(x,y,z)$	Pressure
Re	Reynolds number
t	Underbody height
$u_x(x,y,z)$	Velocity in the x direction
$u_y(x,y,z)$	Velocity in the y direction
$u_z(x,y,z)$	Velocity in the z direction
$u(z)$	Wind velocity at height z
u_*	Friction velocity
U	Total horizontal velocity
v	Train velocity
V	Wind velocity relative to the train
x	Distance along train from train nose
y	Distance perpendicular to track centre line
z	Distance above ground
z_0	Surface roughness length
β	Wind direction relative to track
Ψ	Yaw angle
ρ	Air density
μ	Air viscosity
$\sigma(z)$	standard deviation of wind velocity at height z

Figure 1 Measurements to measure the cross wind forces on the APT using a 1/5th scale model at the Pendine test establishment (4)

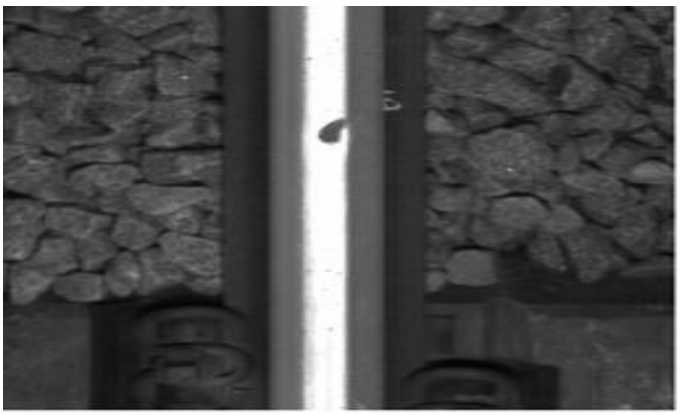

Figure 2 Damage caused to track by ballast being crushed (9)

Figure 3 Sonic anemometer used for slipstream measurements

Figure 4 Pressure probes used for pressure transient measurements

Figure 5 Pressure probes, Cobra probes (for measuring velocity) and force transducers mounted across a high speed railway track (9)

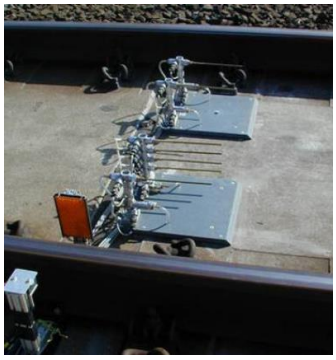

Figure 6 Light gate and pitot probe installation on the track bed (22) (the light gate can be seen in the bottom left of the picture)

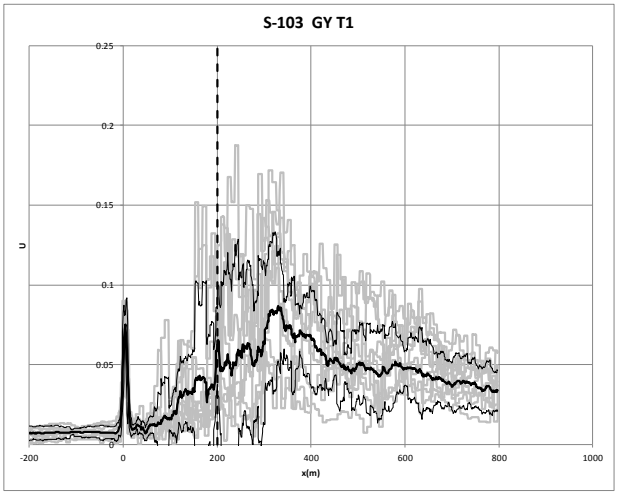

Figure 7 Slipstream velocity measurements at the side of an S103 train (24). The light lines show the individual runs, whilst the solid lines show the ensemble mean and the ensemble mean ± the ensemble standard deviation.

Figure 8 The University of Birmingham moving model (TRAIN) rig

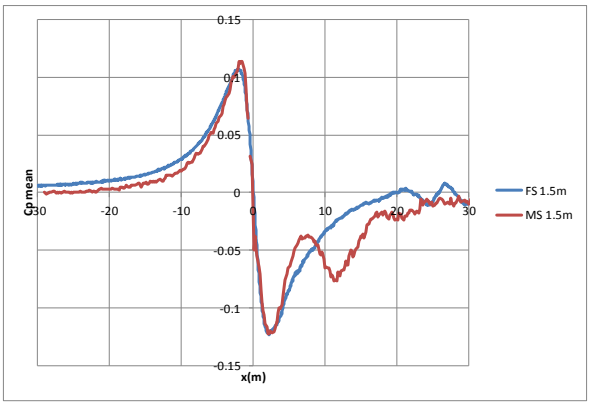

Figure 9 Comparison between nose pressure pulses from full scale (FS) and TRAIN Rig (MS) experiments around an ICE-2 train (27). (The x axis shows the full scale length from the train nose, and the y axis shows pressure coefficient.)

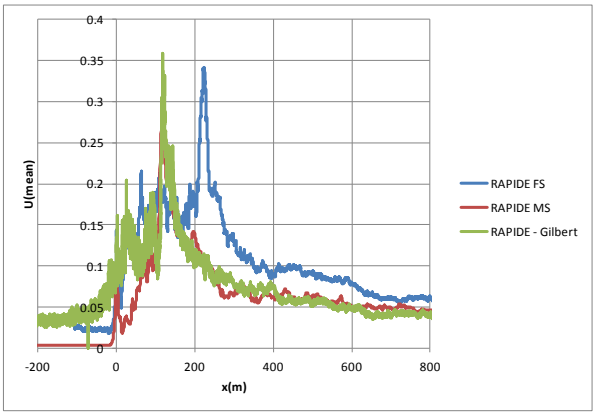

Figure 10 Comparison between slipstream velocity ensembles from full scale (FS) and TRAIN Rig (MS) experiments around an ICE-2 train (27). (The x axis shows full scale length from the train nose, and the y axis shows the horizontal slipstream velocity normalised by train speed. The full scale train is 200m long and the model scale train has a full scale equivalent length of 100m)

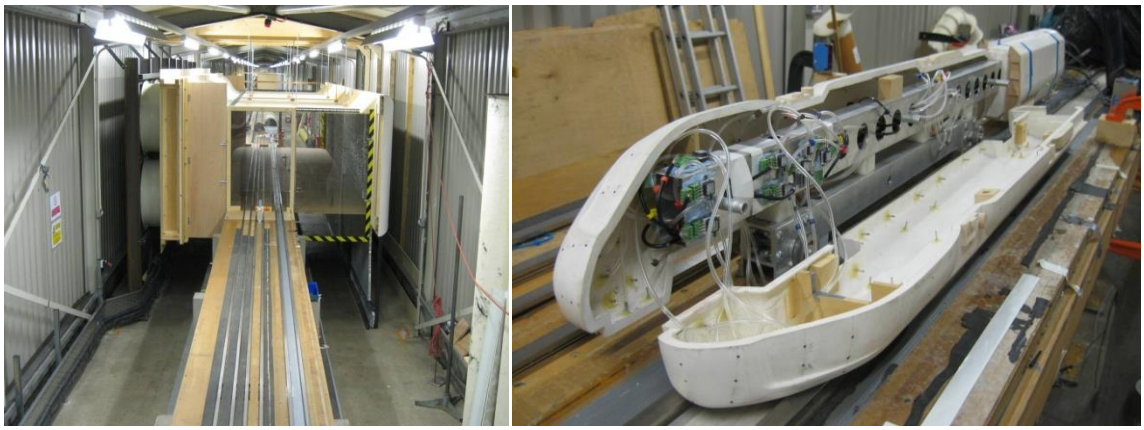

Figure 11 TRAIN Rig cross wind generator and instrumented train showing train mounted pressure transducers (28)

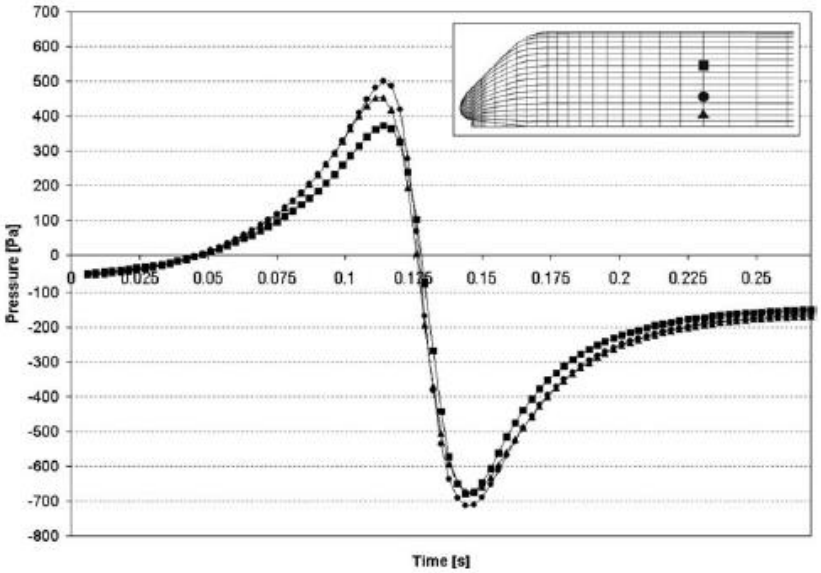

Figure 12 Use of boundary element method to predict nose pressure pulse on the side of a train moving at 250km/hr being passed by another train moving at 275 km/hr (30)

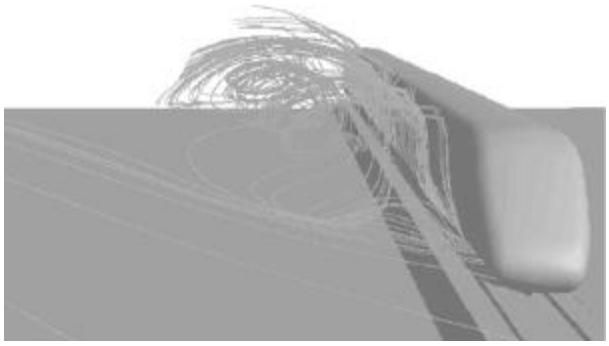

Figure 13 Calculation of train leeside vortex in cross winds using RANS methodology (31)

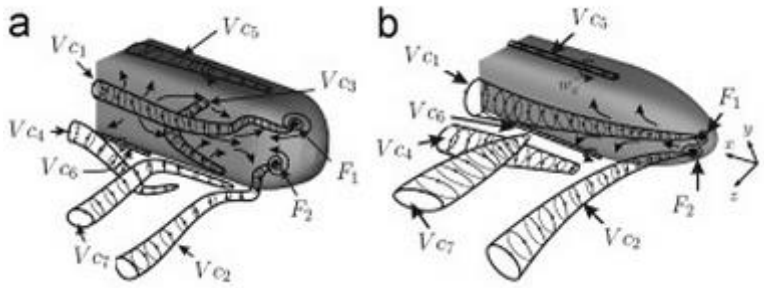

Figure 14 LES simulations of flow structure around a train in cross winds (32)

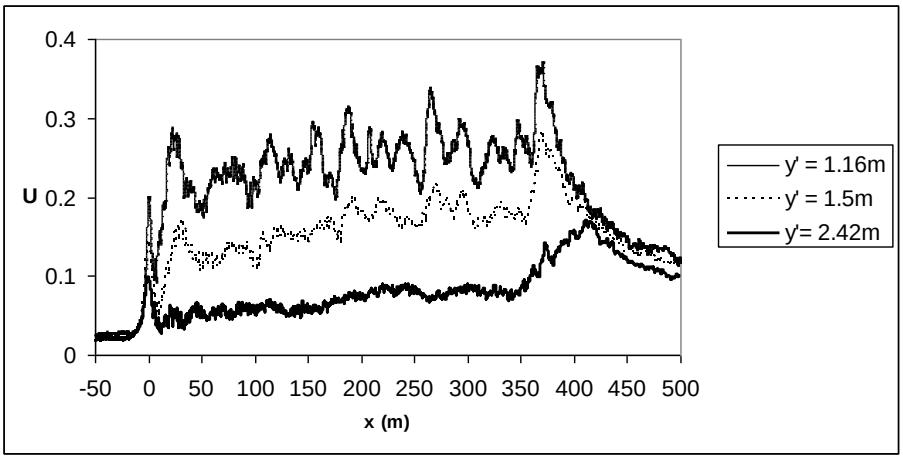

Figure 15. Ensemble average velocities for ICE-2 train (34). (x axis shows distance from the train nose, y axis shows normalised horizontal slipstream velocity, y' is the distance from the centre of the nearest rail i.e. *y*-0.75. Measurements were made at 0.5m height above the top of the rail)

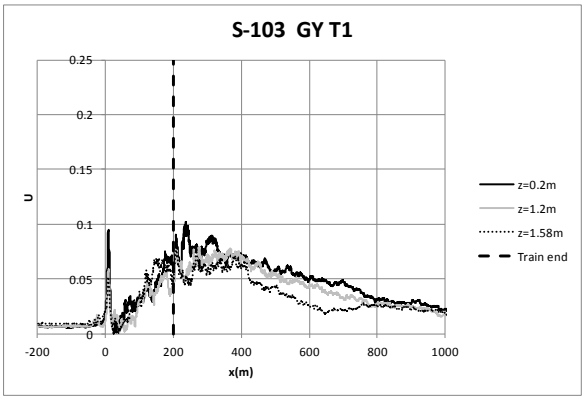

Figure 16 Ensemble average velocities for S-103 Velaro (24). (x axis shows the distance from the train nose, the y axis the normalised horizontal velocity. Measurements were made at the heights shown at a distance of 3.0m from the track centreline. The end of the train is indicated by the vertical dotted line.)

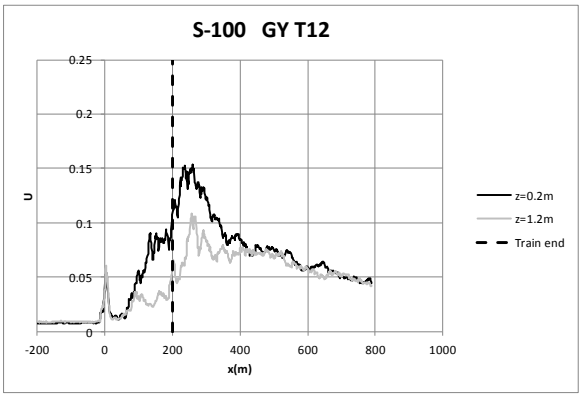

Figure 17 Ensemble average velocities for S-100 TGV (24). (x axis shows the distance from the train nose, the y axis the normalised horizontal velocity. Measurements were made at the heights shown at a distance of 3.0m from the track centreline. The end of the train is indicated by the vertical dotted line.)

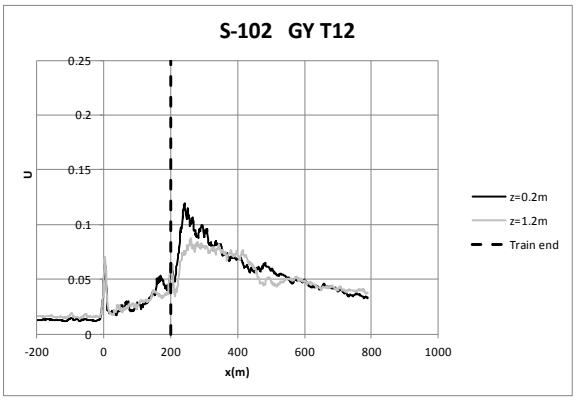

Figure 18 Ensemble average velocities for S-102 (24). (x axis shows the distance from the train nose, the y axis the normalised horizontal velocity. Measurements were made at the heights shown at a distance of 3.0m from the track centreline. The end of the train is indicated by the vertical dotted line.)

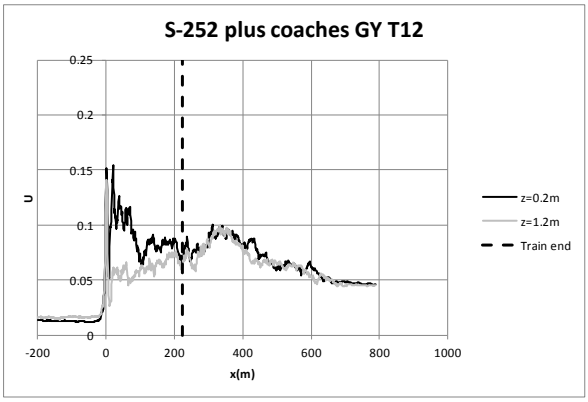

Figure 19 Ensemble average velocities for S-252 locomotive plus coaches (24). (x axis shows the distance from the train nose, the y axis the normalised horizontal velocity. Measurements were made at the heights shown at a distance of 3.0m from the track centreline. The end of the train is indicated by the vertical dotted line.)

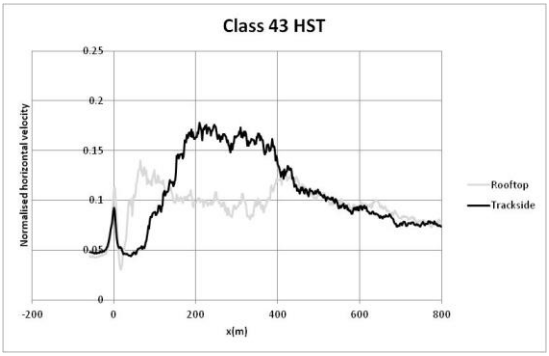

Figure 20 Figure 19 Ensemble average velocities for Class 43 HST. (x axis shows the distance from the train nose, the y axis the normalised horizontal velocity. Measurements were made at trackside at a distance of 3.05m from the track centreline, 0.7m above the top of the rail, and at a point close to the roof top, 4.05m from the track centreline, 4.2m above the top of rail.)

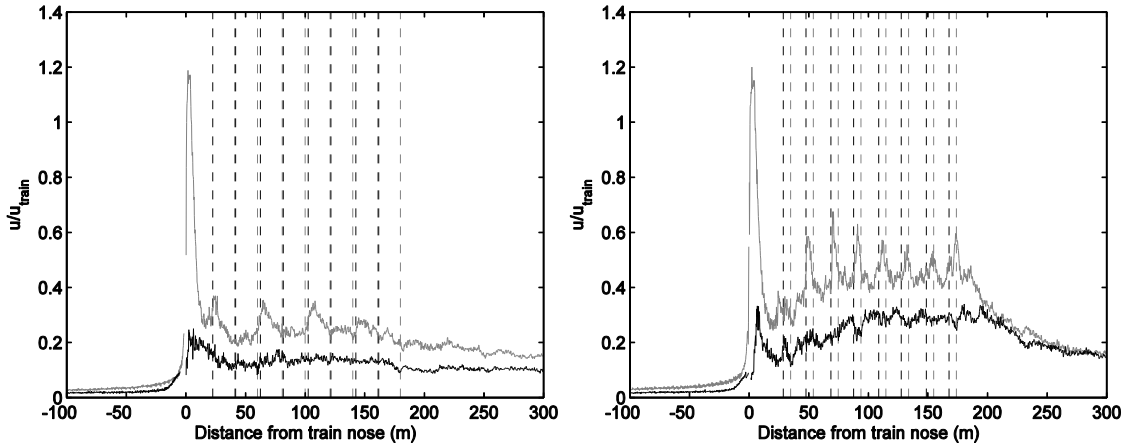

Figure 21 Ensemble average slipstream measurements for a Class 66 locomotive pulling a fully loaded and a 33% loaded container train (35). (x axis shows the distance from the train nose, the y axis the normalised horizontal velocity. Measurements were made at the heights shown at a distance of 1.75m and 3.0m from the track centreline at a height of 2.25m above the top of the rail)

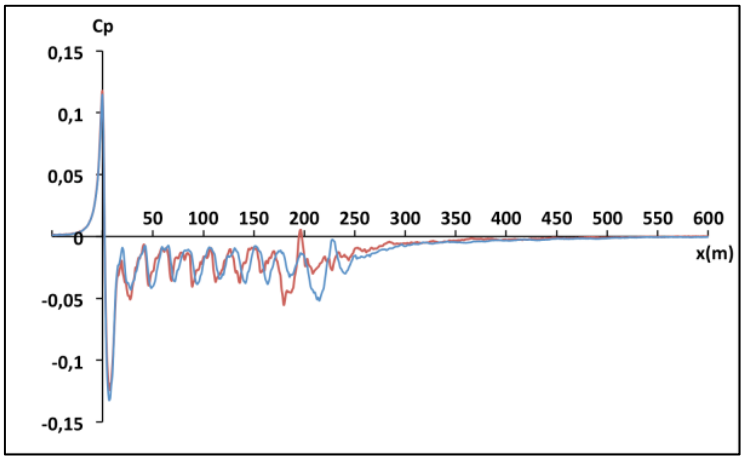

Figure 22 Pressure measurements two HST Class 43 configurations (x axis shows the distance from the train nose, the y axis the pressure coefficient. The blue line is the 2+8 configuration and the red line the 2+7 configuration. Measurements were made at a distance of 2.05m from the track centreline at a height of 1.0m above the top of the rail)

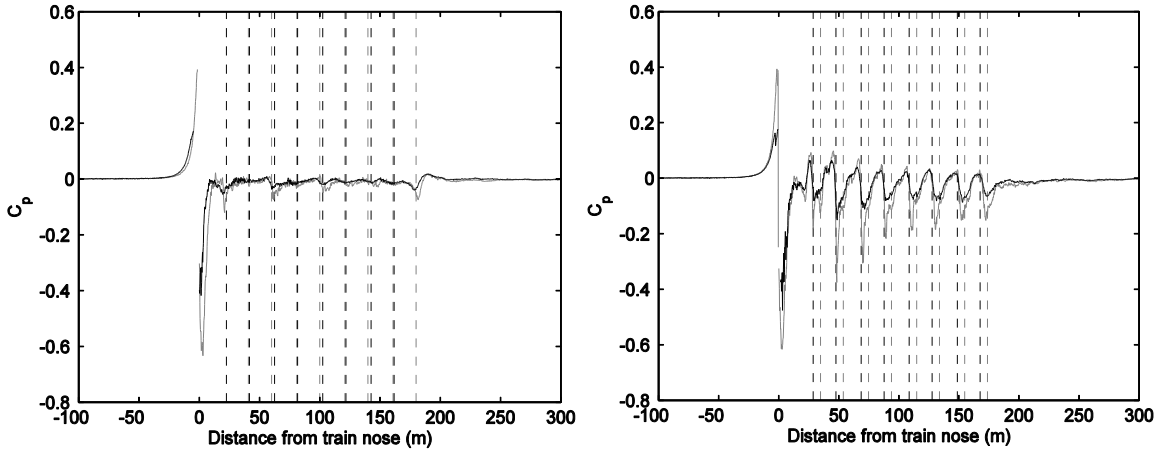

Figure 23 Pressure measurements around a Class 66 locomotive pulling a fully loaded and a 33% loaded container train (35). (x axis shows the distance from the train nose, the y axis the normalised horizontal velocity. Measurements were made at the heights shown at a distance of 1.75m and 3.0m from the track centreline at a height of 2.25m above the top of the rail)

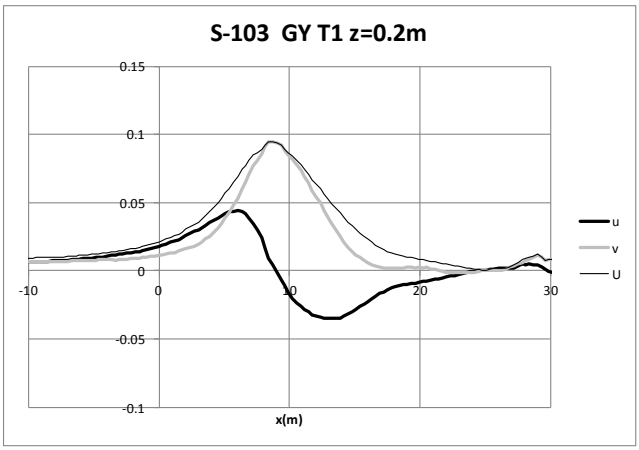

Figure 24. Velocity measurements around nose of Velaro S-103 train (24) (In this figure u is the normalised longitudinal velocity, v is the normalised lateral velocity and U is he normalised overall horizontal velocity

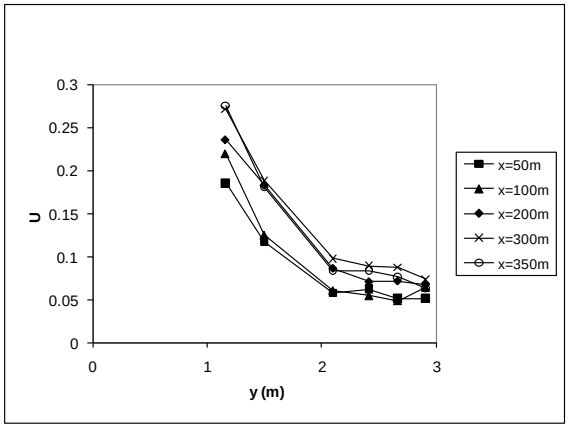

Figure 25 – Boundary layer velocity profiles for the ICE-1 measured 0.5m above the track (34) (The x axis shows the distance from the nearest rail and the y axis the normalised horizontal velocity at different distances from the side of the train, which is 364m long.)

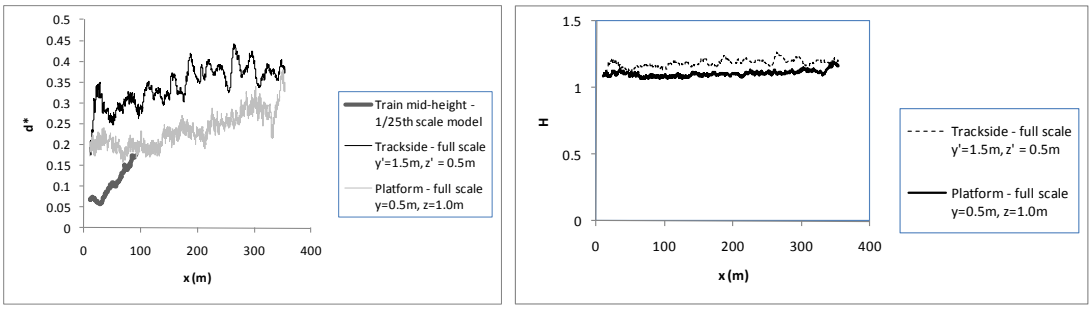

a) Displacement thickness b) Boundary layer form parameter

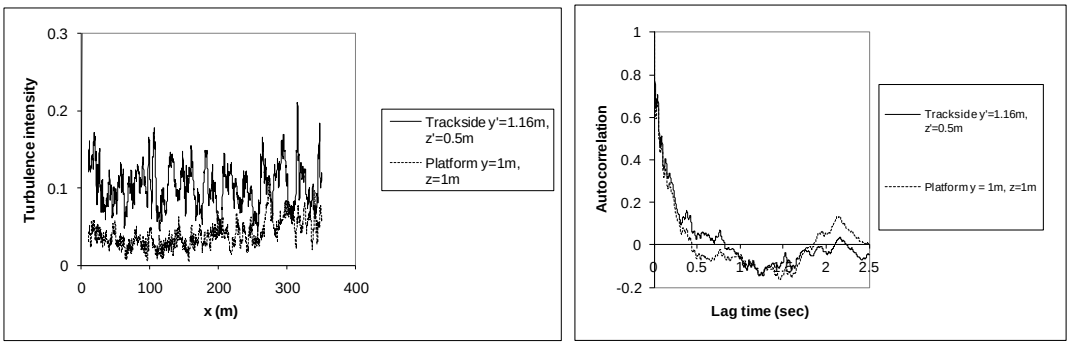

c) Turbulence intensity d) Autocorrelation

Figure 26. Boundary layer parameters and turbulence characteristics for the ICE-1 train measured 0.5m above the track and 0.5m above platform (20) (34)

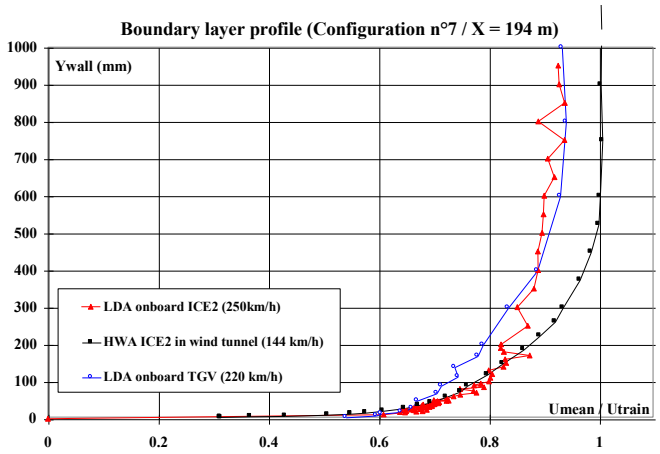

Figure 27. Measurements of train boundary layer from on board LDA (37)

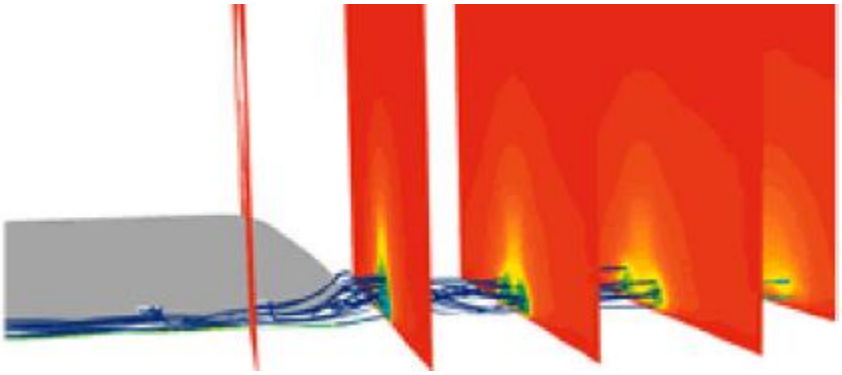

Figure 28. CFD predictions of longitudinal vorticity in the wake of trains (20 from the FLUENT web site)

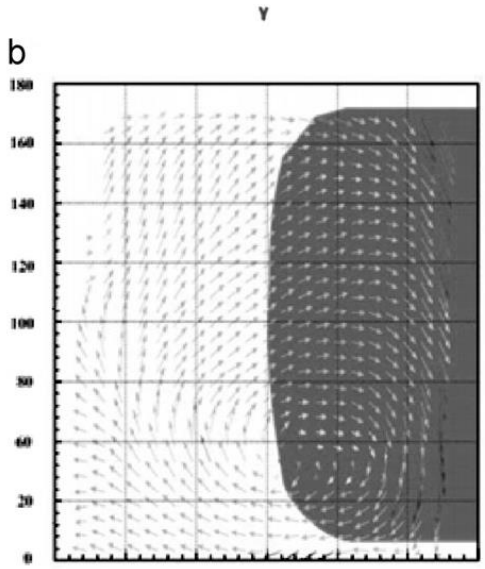

Figure 29. PIV measurements of longitudinal vorticity in the wake of trains (23) (the arrows represent cross flow velocity vectors)

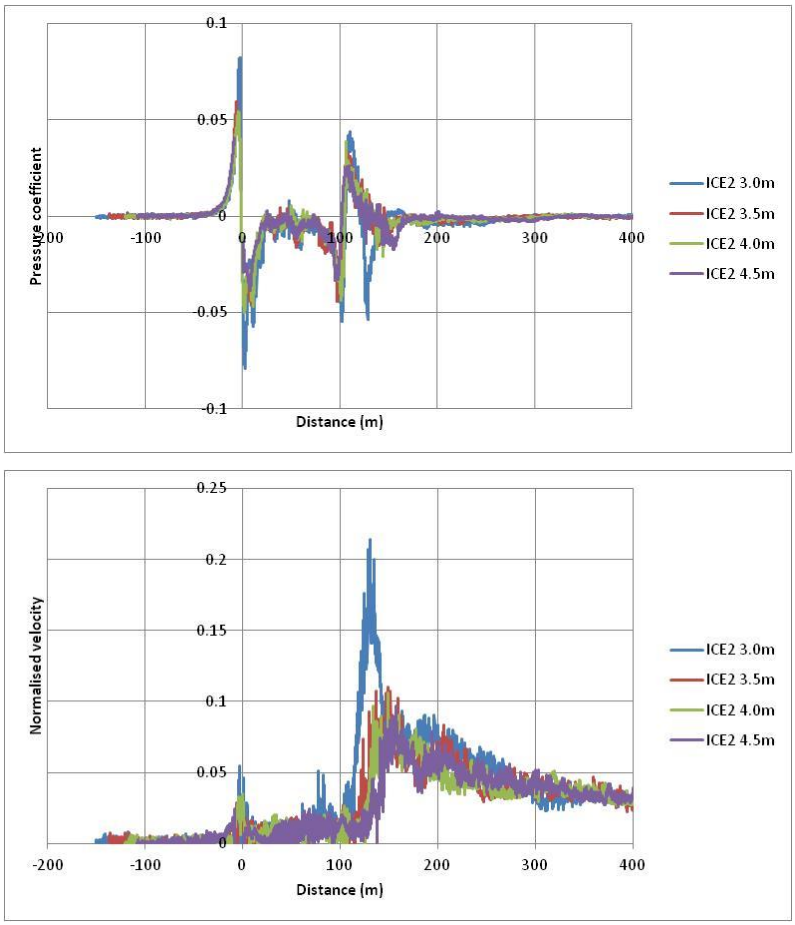

Figure 30. Pressure and slipstream velocity measurements around a 4 car ICE-2 train model (x axis shows distance along the train, y axis shows pressure coefficient or normalised horizontal velocity. The measurements were made 0.2m above the top of the rail, at the indicated distances from the track centre line)

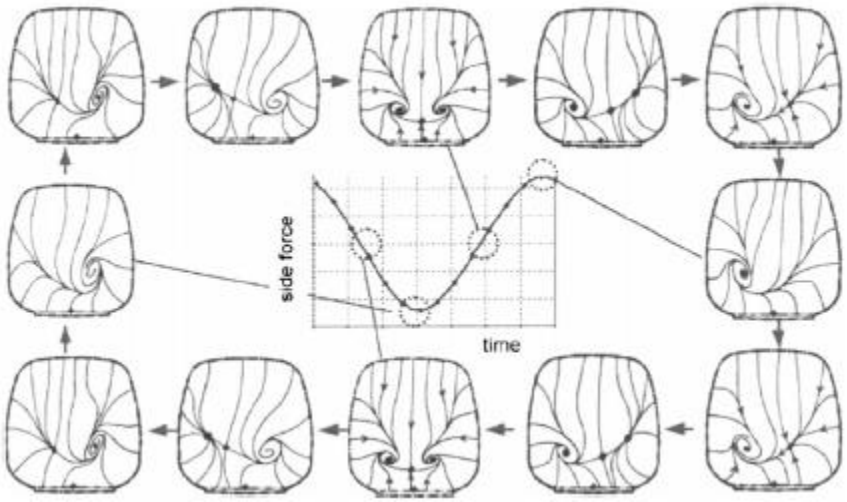

Figure 31. Unsteady RANS CFD calculations of wake unsteadiness (38)

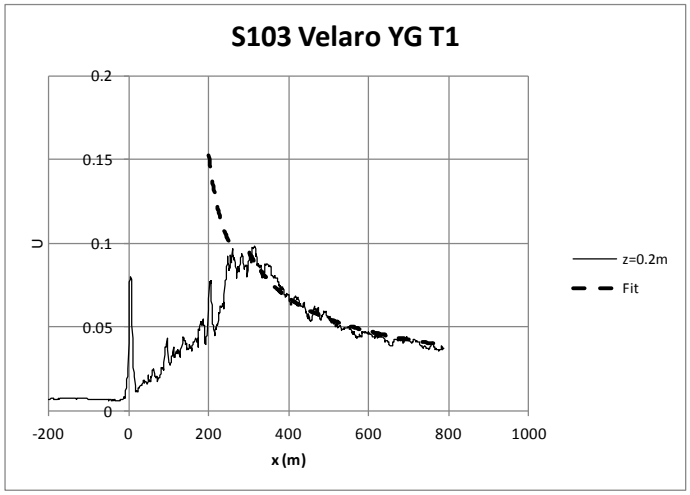

Figure 32. Velocity decay in the wake of the S-103 Velaro (24)

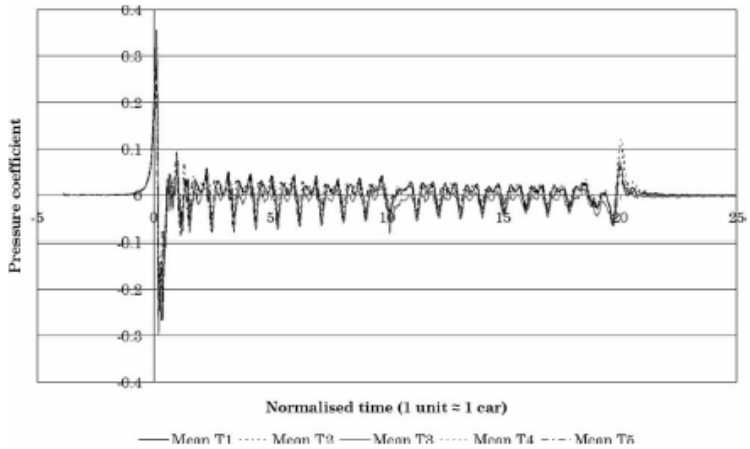

Figure 33 Ensemble average pressure coefficients beneath a 20 car Class 373 Eurostar at different points across the track (8) (The x axis shows distance along the train normalised with the length of an average car, and the y axis shows a pressure coefficient)

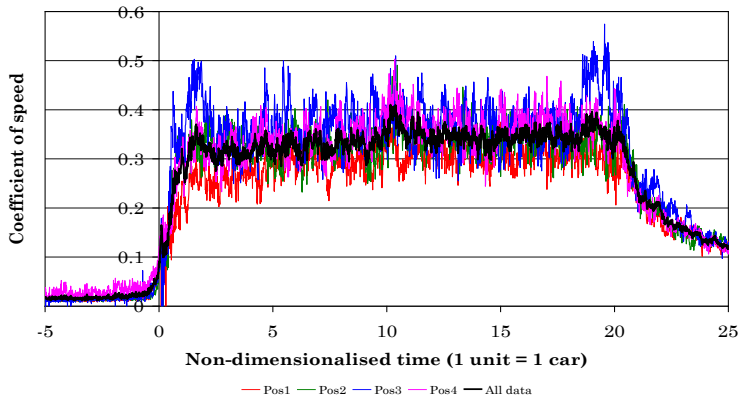

Figure 34 Ensemble average normalised velocities beneath a 20 car Class 373 Eurostar at different points across the track (9) (The x axis shows distance along the train normalised with the length of an average car, and the y axis shows horizontal velocity normalised with train speed.)

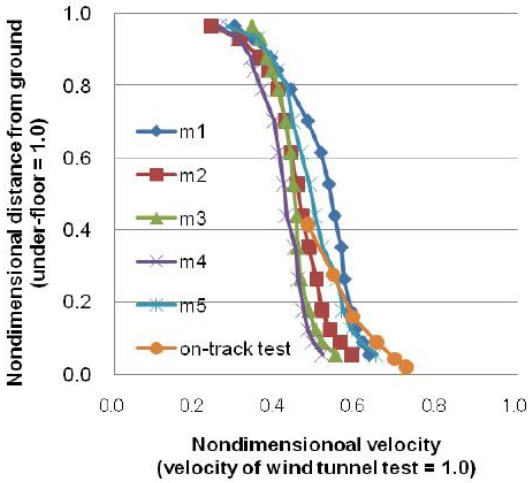

Figure 35 Velocity profiles across the underbody gap beneath a Shinkansen train (40) (x axis shows velocities normalised by train velocities at different distances down the track, whislt the y axis shows the distance above the track normalised with the underbody gap height.

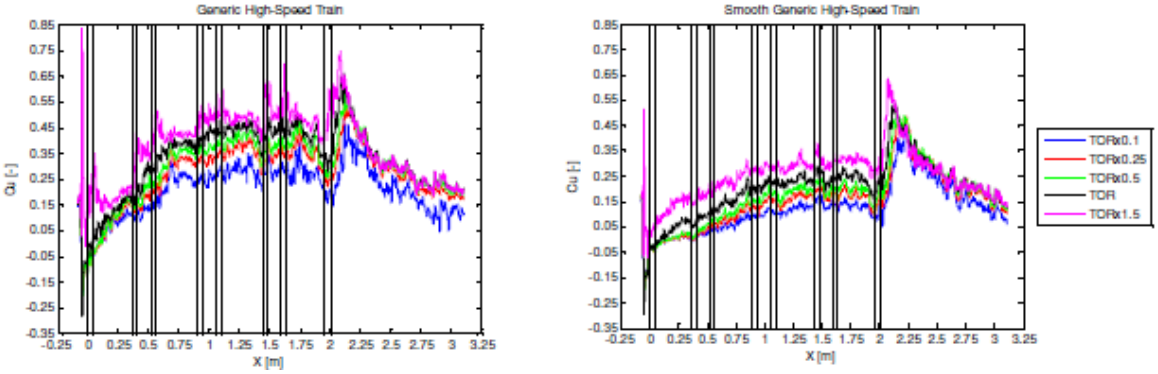

Figure 36. Velocity profile evolution in the underbody region along two generic high speed train models (41) (The left hand figure shows the results for a generic high speed train, and the right hand figure for a similar train with a smooth underbody. The x axis is the distance along the model train, and the y axis is the normalised horizontal velocity at different heights above the top of the rail TOR)

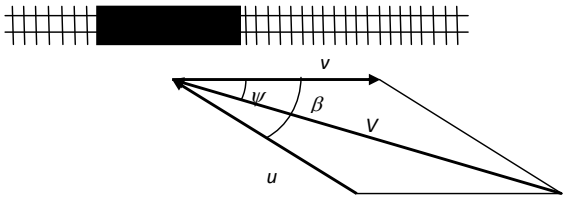

Figure 37 Velocity vector diagram for a train in a cross wind

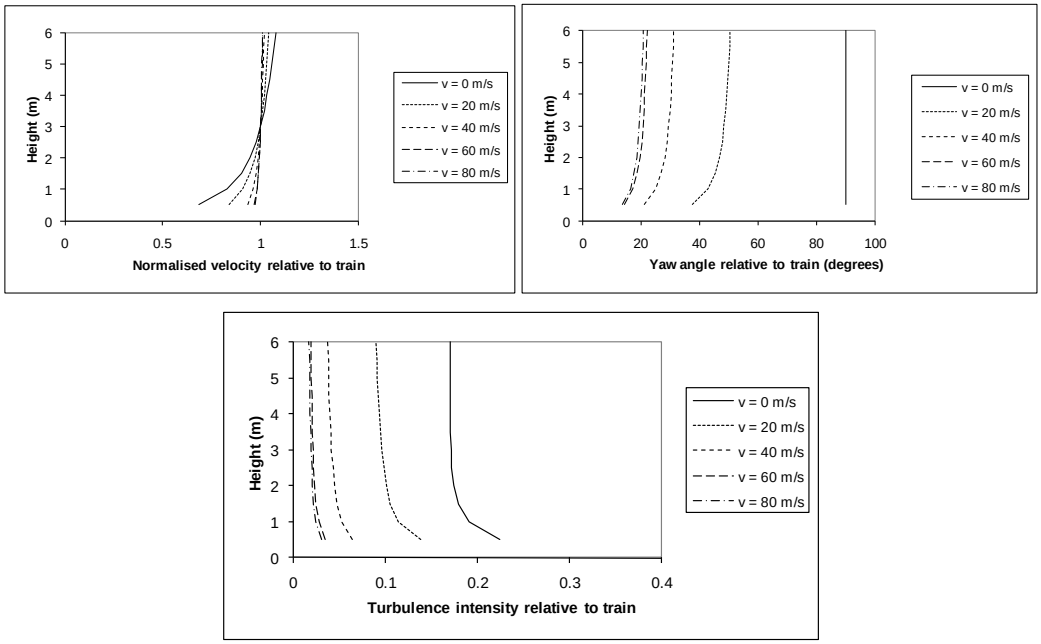

Figure 38 Wind parameters relative to a moving train (20)

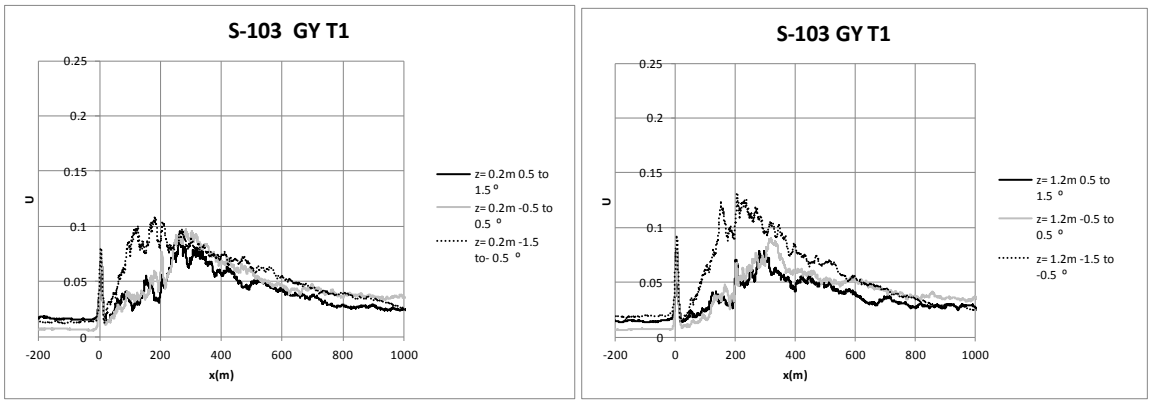

Figure 39 Effect of cross winds on ensemble average velocities of Velaro S-103 (24) (Left hand figure shows velocities measured at 0.2m above the top of the rail. Right hand figure shows velocities measured 1.2m above top of rail, x axis is distance along the train, and y axis is normalised horizontal velocity for different yaw angle ranges

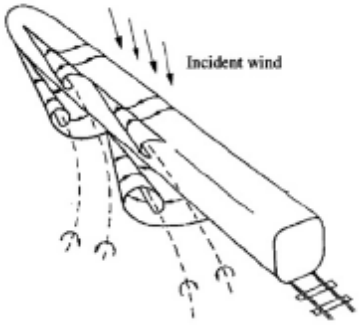

Figure 40. Flow around an idealised train (44), (45)

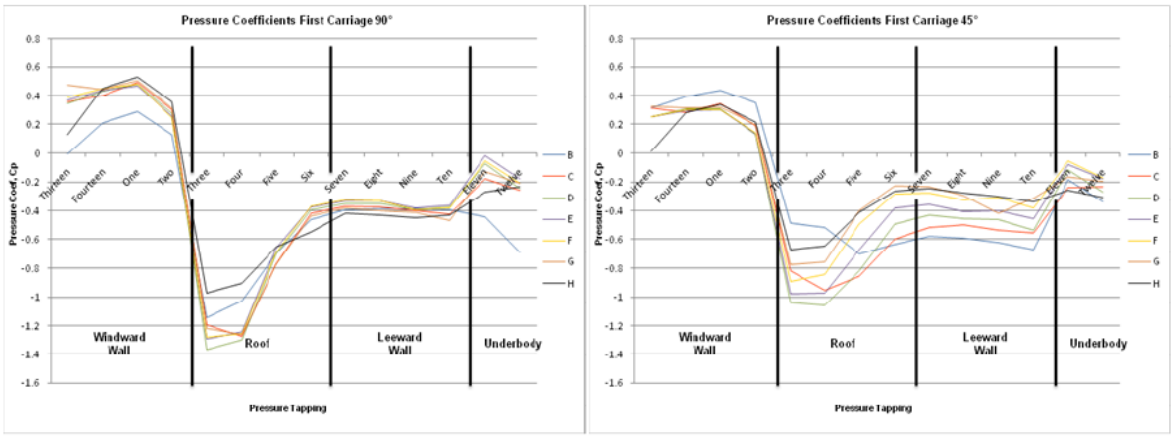

Figure 41 Variation of mean pressure coefficient on the first car of a two car class 365 EMU. (46) (The different lines indicate different sections along the train, section B being closest to the nose, and section H furthest away)

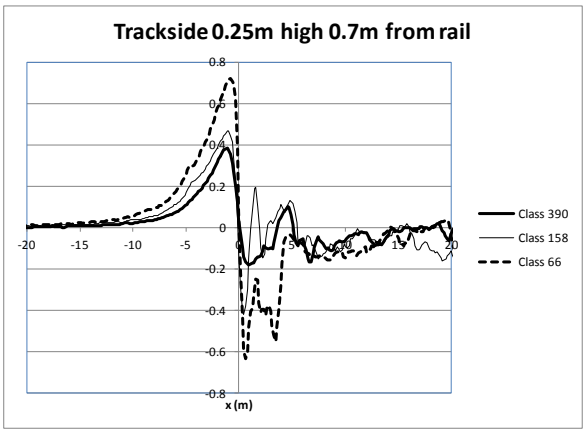

Figure 42 Pressure measurements on hoardings at the side of the track during the passage of trains of different types (47) (48) (The x axis shows relative position of the train nose to the measurement position, and the y axis shows pressure coefficient)

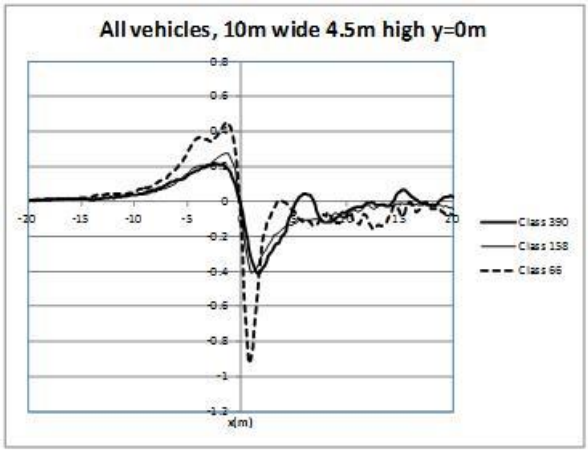

Figure 43 Pressure measurements on an overbridge above the track during the passage of trains of different types (47) (48) (The x axis shows relative position of the train nose to the measurement position, and the y axis shows pressure coefficient)

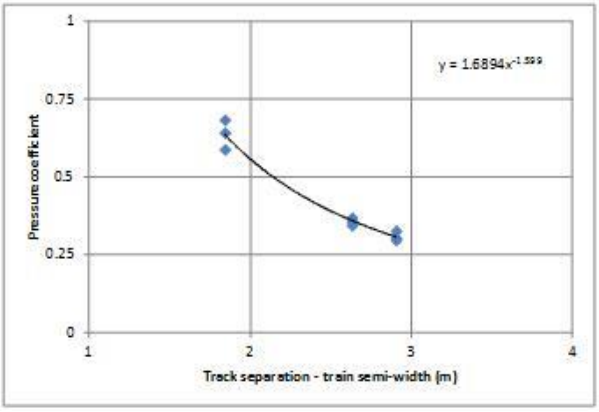

Figure 44 Peak to peak nose pressure measurements on an ETR 500 train passed by another ETR-500 train (49) (the x axis shows the track separation minus the train semi-width and the y axis shows the pressure coefficient)

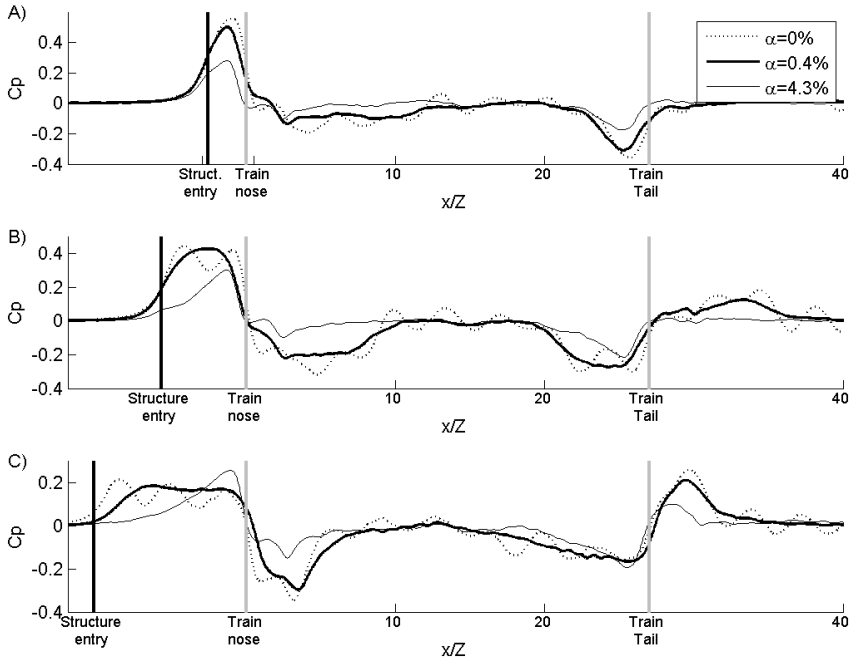

Figure 45 Static pressure variations for ICE-2 model passing through a box tunnel with different degrees of confinement (50) (51) (Measurements on the tunnel wall 0.26 of the tunnel height above the track, the top, middle and bottom figures show measurements at 20, 45 and 80% of the tunnel length respectively. The x axis shows position of train relative to measuring point and the y axis shows the pressure coefficient. The different curves show the percentage of leakage area to tunnel wall area)

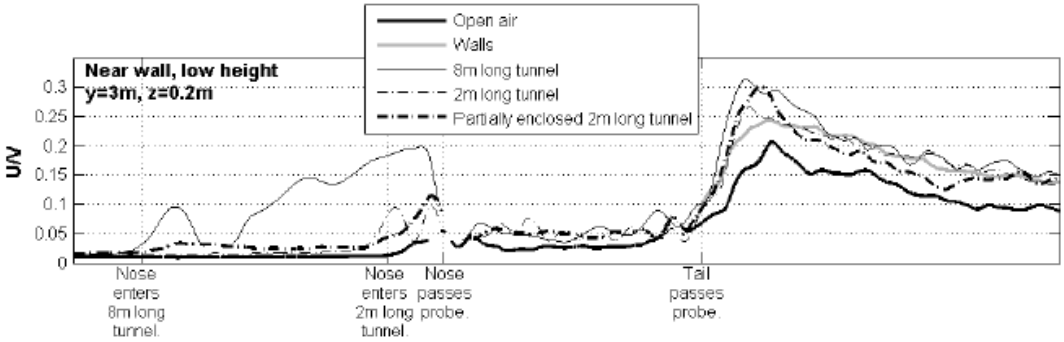

Figure 46 Velocity variations for ICE-2 model in the open air, passing walls and travelling through tunnels (50) (52) (The x axis shows position of train relative to measuring point and the y axis shows the pressure coefficient.)

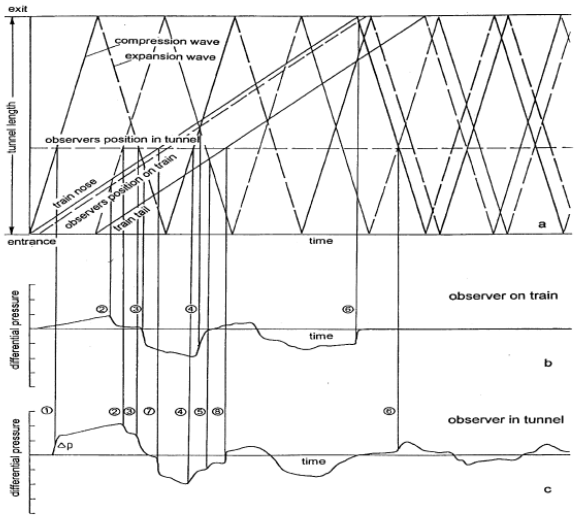

Key

1 Initial head wave
2 Initial tail wave
3 1. Reflection head wave
4 2. Reflection head wave
5 1. Reflection tail wave
6 Exit wave
7 Passing of head
8 Passing of tail

Figure 47 Wave diagram for single train in tunnel (12)

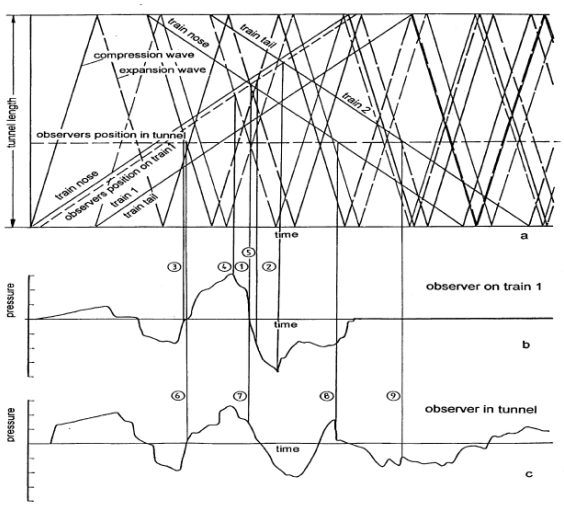

Additional waves from second train

Key

1 Passing of head of train 2
2 Passing of tail of train 2
3 Initial head waves of train 2
4 Initial tail waves of train 2
5 1. Reflection head wave train 2
6 Initial head wave train 2
7 Initial tail wave train 2
8 Passing of head train 2
9 Passing of tail train 2

Figure 48 Wave diagram for double train in tunnel (12)